QED Effects on Inner Shells of Heavy Atoms

W. R. Johnson*

Department of Physics, University of Notre Dame, Notre Dame, IN 46556, USA

Abstract Experimental values of the Lamb shift of $1s$ electrons in heavy atoms are obtained by comparing experimental K-shell binding energies with careful atomic-structure calculations. These experimental values agree with numerical calculations of the strong-field one-loop Lamb shift to about 5%. Similar tests of the strong-field Lamb shift for $n = 2$ and $n = 4$ states, obtained by comparing spectra of highly-charged ions with precise many-body calculations, are also described and discussed.

1 Introduction

In this paper, we describe many-body calculations of binding energies of K-shell electrons in heavy atoms and show how these calculations, when combined with experimental measurements, permit one to infer the $1s$ Lamb-shift at the 5% level of accuracy. Theoretical attempts to understand K-shell binding energies in heavy atoms were initiated in the seminal work of Brenner and Brown [1] more than forty years ago. The first section of this paper is an updated version of a review paper on this subject by Johnson and Cheng. [2]

The experimental binding energy of a K-shell electron in a heavy atom is approximately equal to the Dirac-Coulomb energy of a $1s$ electron bound to a point nucleus. The difference between the one-electron Dirac energy and the experimental K-shell binding energy ($\approx$ 10keV for nuclear charges Z in the range 70–90) is accounted for by nuclear finite size, the electron-electron Coulomb interaction, and the Breit interaction. We discuss each

*This work was supported in part by NSF Grant #PHY-9513179.

of these factors in turn and compare the resulting atomic structure calculations with experiment. The differences between experimental binding energies and those obtained from atomic structure calculations are attributed to the omitted radiative corrections. These differences are used to infer "experimental" values for the $1s$ Lamb shift. The resulting experimental values are compared with theoretical calculations of the strong-field Lamb shift and found to agree to about 2%. Given the error in the atomic structure calculations caused by omitting correlation corrections and the error in the theoretical Lamb shift caused by omitting higher-order radiative corrections, we estimate that the comparison confirms the numerical calculations of the $1s$ Lamb shift to about 5%.

We next turn to a discussion of the Lamb shift in the $n = 2$ shell of highly-charged uranium ions inferred by comparing observed spectra with relativistic many-body calculations. The experimental and theoretical values of the $n = 2$ Lamb-shift for these ions agree to about 5%. Finally, we compare third-order many-body perturbation theory (MBPT) calculations with experimental valence energies in copperlike ions to infer experimental values of the $n = 4$ Lamb-shift. For these ions, one finds agreement between the calculated and experimental Lamb shift to about 10%.

2 K-shell Binding Energy

In Fig. 1, we plot experimental values of K-shell binding energies in Ry from the tabulation of Bearden and Burr [3] against nuclear charge for atoms with $Z \geq 20$. The experimental values were obtained by combining measurements of photoionization thresholds and inner-shell X-rays. The typical accuracy given for the experimental K-shell energies is 0.05 Ry, which is much smaller than the size of the dots on the graph. For comparison, we also plot the Dirac-Coulomb energy of a $1s$ electron on the same graph to illustrate the extent to which the one-electron picture of the K-shell electron describes the binding.

2.1 Electron-nucleus Coulomb interaction

As seen in Fig. 1, the Dirac-Coulomb $1s$ energy

$$\epsilon_{1s} = \frac{2Z^2}{1 + \sqrt{1 - \alpha^2 Z^2}}, \tag{1}$$

accounts for the K-shell binding energies qualitatively. To include corrections for finite nuclear size, one replaces the Coulomb potential by the po-

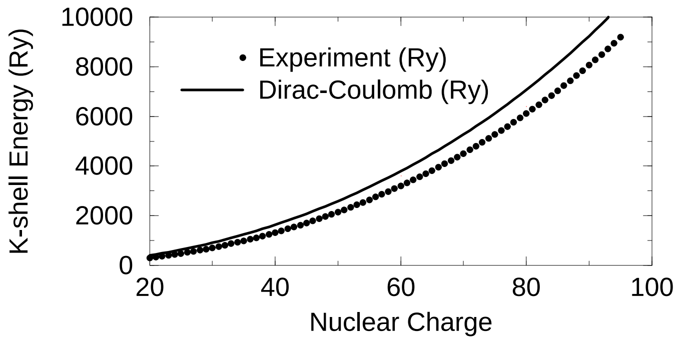

Figure 1: Experimental K-shell binding energies [3] compared with the $1s$ Dirac-Coulomb energy (Ry).

tential of a spherically symmetric charge distribution

$$\frac{Z}{r} \rightarrow \int \frac{\rho_{\rm nuc}(r')d^3r'}{|\boldsymbol{r}-\boldsymbol{r}'|}. \tag{2}$$

In the calculations described here, the nuclear charge distribution is assumed to have the form

$$\rho_{\rm nuc}(r) = \frac{\rho_0}{1+\exp\left[(r-C)/a\right]}, \tag{3}$$

where the parameters C and a are inferred from e-nucleus scattering experiments [4] or from studies of muonic X-rays [5]. The K-shell energies are most sensitive to the root-mean-square radius of the charge distribution. For some heavy atoms such as Rn, experimental values of the nuclear radii are not available and one must rely on empirical radii obtained by fitting the experimental data. Such a fit, illustrated in Fig. 2, was given in Ref. [6]. As a specific example, the Coulomb and nuclear-size corrections to the K-shell energy of Hg (Z=80) are 7064.38 and -4.03 Ry, respectively, giving a total of 7060.36 Ry, which can be compared with the experimental binding energy in Hg of 6108.44(6) Ry. We see that, although the finite nuclear-size corrections are large compared to the experimental uncertainty, they account for only a tiny fraction of the non-Coulomb energy. In the calculations to follow, nuclear finite size is included in the definition of the electron-nucleus potential.

2.2 Electron-electron Coulomb interaction

The dominant correction to the one-electron energy is from inter-electron Coulomb interactions. These interactions are well described in the Hartree-Fock approximation. The many-electron wave function is represented as an

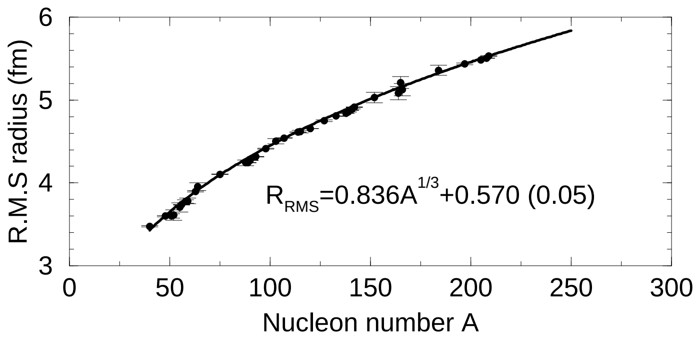

Figure 2: Nuclear root-mean-square radii. The solid curve is a fit to the experimental data from [6].

antisymmetric product of one-electron orbitals $\phi_a(\boldsymbol{r})$ satisfying the (Dirac) HF equations

$$(H_{\rm Dirac} + V_{\rm HF})\phi_a = \epsilon_a \phi_a, \tag{4}$$

with

$$\begin{aligned} V_{\rm HF}\ \phi_a(\boldsymbol{r}) = & \sum_b \int \frac{d^3r'}{|\boldsymbol{r}-\boldsymbol{r}'|}\phi_b^\dagger(\boldsymbol{r}')\phi_b(\boldsymbol{r}')\phi_a(\boldsymbol{r}) \\ & - \sum_b \int \frac{d^3r'}{|\boldsymbol{r}-\boldsymbol{r}'|}\phi_b^\dagger(\boldsymbol{r}')\phi_a(\boldsymbol{r}')\phi_b(\boldsymbol{r}). \end{aligned} \tag{5}$$

These equations are solved self-consistently for all occupied orbitals a. The negative of the DHF eigenvalue $-\epsilon_a$ is the "frozen-core" approximation to the removal energy of an electron with quantum numbers a. Returning to the Hg example above, where the experimental binding energy is 6108.44(6) Ry, one finds that the DHF energy for a $1s$ electron is $-\epsilon_{1s} = 6148.45$ Ry, giving a -911.90 Ry correction to the electron-nucleus energy. Even though the dominant part of the K-binding energy is accounted for by the DHF energy, ≈ 500 eV is still missing.

2.3 Relaxation and correlation

Within the independent particle framework, the K-shell binding energy is the difference of the DHF energies of the ion and atom,

$$E_{1s} = E_{\rm ion} - E_{\rm atom}. \tag{6}$$

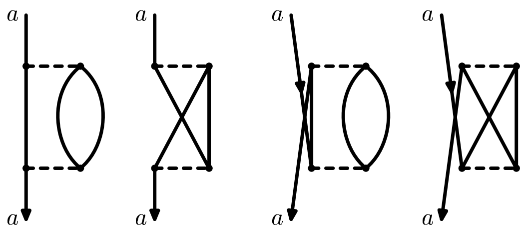

Figure 3: Second-order relaxation and correlation diagrams for a hole in subshell a.

As mentioned in the previous paragraph, $E_{1s} = -\epsilon_{1s}$ is the "frozen-orbital" approximation, in which differences between the atomic and ionic orbitals are ignored. In actual calculations, the ionic orbitals differ from the atomic orbitals, so E_{1s} differs from the frozen core value,

$$E_{1s} = -\epsilon_{1s} + \Delta_{1s}, \tag{7}$$

where Δ_{1s} is the contribution associated with the difference in orbitals. The correction Δ_{1s} is referred to as the rearrangement or relaxation energy. For the example of Hg discussed above, $\Delta_{1s} = -7.01$ Ry.

The K-shell binding energy can, alternatively, be obtained from MBPT, as explained in Ref. [7], treating the ion as a hole in subshell a of the closed-shell atom. From this point of view, the lowest-order energy is $-\epsilon_a$ and the diagrams in Fig. 3 give the second-order corrections to the energy. The first two of these diagrams are dominated by the second-order approximation to Δ_a. Third- and higher-order MBPT diagrams are similarly dominated by the third- and higher-order contributions to Δ_a. The remaining parts of the first two diagrams in Fig. 3, together with the second two diagrams give second-order correlation contributions to the K-shell binding energy having the value ≈ 0.1 Ry, nearly independent of Z. These correlation corrections are ignored here, but have been studied theoretically in the Ref. [8], and have been recently included in calculations of X-ray energies in Ref. [9].

2.4 Breit interaction

The diagrams of Fig. 4 represent the contribution to the energy caused by exchange of a transverse photon between electrons. The first of these diagrams vanishes by symmetry for a closed-shell atom. The second (exchange) term does not vanish. In the static limit, this diagram is just the exchange

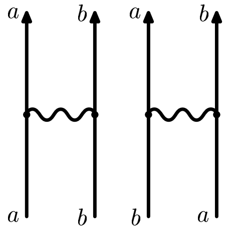

Figure 4: Transverse photon exchange.

matrix element of the Breit operator:

$$b_{12} = -\frac{\boldsymbol{\alpha}_1 \cdot \boldsymbol{\alpha}_2 + \boldsymbol{\alpha}_1 \cdot \hat{r}_{12}\, \boldsymbol{\alpha}_2 \cdot \hat{r}_{12}}{2r_{12}}. \tag{8}$$

The Breit interaction is easily generalized to include the retardation of the transverse photon interaction, as explained, for example, in Ref. [10]. The Breit contribution to K-shell binding energies, including relaxation, is the difference between the Breit energies of the atom and ion. For the example case of Hg, the relaxed static Breit interaction is -22.29 Ry. Including retardation reduces this value by 0.45 Ry, leading a value of 6119.59 Ry for the K-shell energy. This value includes electrostatic, magnetic, and retardation corrections; it is expected to be accurate to about 0.1 Ry.

In Fig. 5, we plot the differences between experimental K-shell binding energies and theoretical energies determined as described above. We expect these differences to reflect the omitted self-energy, vacuum-polarization, and higher-order radiative corrections. Indeed, we use the differences shown in Fig. 5 to define "experimental" values of $1s$ Lamb shift. These experimental values will be compared with theoretical calculations of the Lamb shift in the following subsection.

2.5 Self-energy expansion

As pointed out previously, the K-shell binding energy is dominated by the relativistic one-electron interaction with the nucleus. We expect that the radiative corrections will be similarly dominated by the one-electron radiative corrections; the self-energy and vacuum polarization. The self-energy can be written in terms of a dimensionless factor $F(Z\alpha)$ as

$$\Delta E_{1s} = \frac{\alpha}{\pi}(\alpha Z)^4 F(Z\alpha)\, mc^2, \tag{9}$$

where the function $F(Z\alpha)$ can be expanded in powers of αZ as

$$F(Z\alpha) = A_4 + (\alpha Z)\, A_5 + (\alpha Z)^2 A_6 + \cdots\,. \tag{10}$$

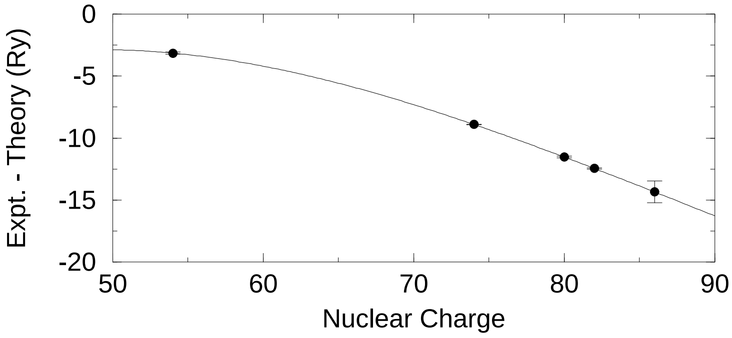

Figure 5: Difference between experimental and theoretical K-shell energies as a function of Z. The differences define the "experimental" $1s$ Lamb shift.

The leading few terms in this expansion are:

$$A_4 = \frac{4}{3}\left[\ln(Z\alpha)^{-2} + \frac{5}{6} - 2.9841285\right], \tag{11}$$

$$A_5 = 3\pi\left[1 + \frac{11}{128} - \frac{1}{2}\ln 2\right], \tag{12}$$

$$A_6 = \left[7\ln 2 - \frac{63}{80}\right]\ln(Z\alpha)^{-2} - \frac{3}{4}\ln^2(Z\alpha)^{-2} - 33.2. \tag{13}$$

If this expansion converged for large Z, contributions from the higher-order terms could be used to give reliable values of the self energy for heavy atoms. This is not the case, however, as shown in Fig. 6, where we plot the successive contributions to $F(Z\alpha)$ against Z.

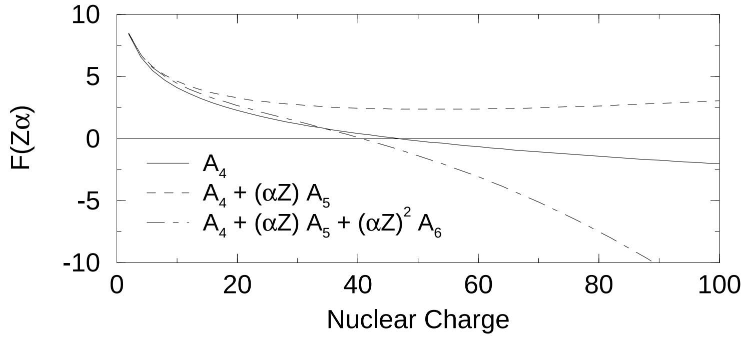

Figure 6: Contributions to $F(Z\alpha)$ from successive orders of αZ in the external-field expansion.

2.6 Non-perturbative $1s$ self-energy

In light of the obvious lack of convergence of the series expansion for nuclear charges of interest in the study of K-shell binding energies, it is necessary to turn to non-perturbative (in αZ) calculations. The earliest such study was that of Brown *et al.* [11], who gave a decomposition of the self-energy suitable for numerical eveluation. The formulation was sound, but the numerical implementation by Brown and Mayers [12] contained errors and the resulting numerical value of the $1s$ self-energy for Hg was incorrect. Desiderio [13] gave the first accurate numerical values for the self-energy of a $1s$ electron in the Coulomb field of a nucleus with Z in the range 70–90. Several years later, Mohr [14] obtained precise values of the $1s$ self-energy for ions with nuclear charges in the range $Z = 10$–100. Finite nuclear size and an atomic screening potential were included in the self-energy by K. T. Cheng, [15], and the self-energy with finite nuclear size corrections was also evaluated by Soff *et al.* [16]. In recent years, improved numerical methods for evaluating the self-energy have been developed in Refs. [17–19]. We show results of some of the non-perturbative calculations of $F(Z\alpha)$ in Fig. 7.

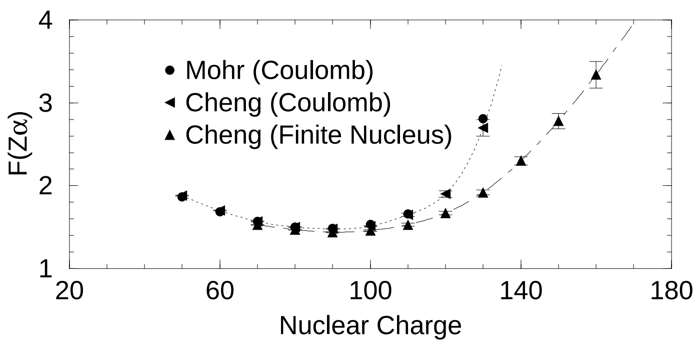

Figure 7: Numerical Calculations of the $1s$ self energy in a Coulomb field [14,15] and including nuclear finite size. [15]

2.7 Test of Lowest-Order QED

Now let us consider the lowest-order QED corrections for a $1s$ electron; the self-energy and vacuum-polarization. We use the numerical values of [15] to evaluate the self-energy and we approximate the vacuum-polarization by the expectation of the Uehling potential. The resulting theoretical values of the QED corrections are listed in the last column of Table 1, where they are compared with the "experimental" QED corrections discussed previously. The experimental and theoretical QED corrections are found to agree to

Table 1: "Experimental" vs. Theoretical QED.

Atom	Expt.	Theory	Diff.	QED
Xe	2540.28(8)	2543.43	-3.15(8)	-3.22
W	5110.42(2)	5119.03	-8.61(2)	-8.73
Hg	6108.44(6)	6119.59	-11.15(6)	-11.36
Pb	6468.71(5)	6480.83	-12.11(5)	-12.35
Rn	7232.73(89)	7247.07	-14.34(89)	-14.51

about 2%. This level of agreement is fortuitous, however, since we have neglected correlation corrections to the structure and higher-order corrections to the $1s$ Lamb shift. The former corrections amount to 1–2% of the Lamb shift and the latter are about 1%. We conclude that QED corrections to the $1s$ state are tested at the 5% level by these studies of K-shell binding energies.

3 Outer Shells of Highly-Charged Ions

It is of interest to compare the inner shell tests of QED described above with tests in outer shells of highly-charged ions. Below, we consider two such tests, one in U ions in the first row of the periodic table, and a second in copperlike ions.

3.1 Highly-Charged Uranium Ions

Beiersdorfer *et al.* [20] measured $2p_{3/2} - 2s_{1/2}$ transition energies in uranium ions having 3 to 10 electrons in a high-energy electron beam ion trap. An example of the transitions considered is the $2s^2 2p^2_{1/2}|_{J=0}$–$2s2p^2_{1/2}2p_{3/2}|_{J=1}$ transition in carbon-like uranium. Comparing the experimental energies of such transitions with MBPT calculations leads to "experimental" values of the $n = 2$ Lamb shift that can be also used to test strong-field QED.

An analysis of these experiments was carried out using second-order MBPT and compared with lowest-order QED corrections in Ref. [21]. The MBPT calculations and the QED calculations were carried out in a common local model potential chosen to give a rapidly converging perturbation expansion. Typical diagrams occurring in the MBPT calculation are shown in Fig. 8; those on the top row are correlation diagrams and those on the lower row are second-order Hartree-Fock counter terms.

The first- and second-order Coulomb $E^{(k)}$ and Breit $B^{(k)}$ corrections to the $2p_{1/2} - 2s_{1/2}$ energy difference in a.u. for three of the ions are listed in

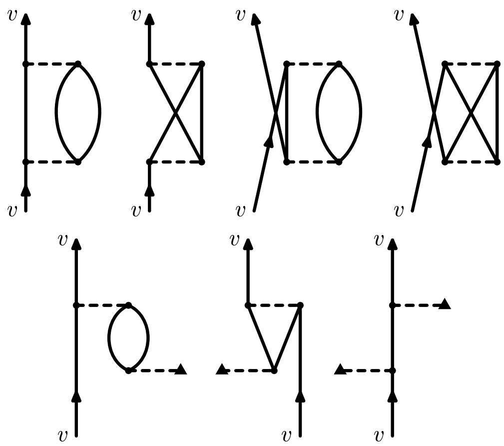

Figure 8: Second-order MBPT for an ion with one valence electron.

Table 2. The first-order Breit correction $B^{(1)}$ includes retardation. The line labeled "Recoil" gives reduced-mass and mass-polarization corrections. For each of the three cases, the MBPT series appears to be rapidly converging.

Table 2: MBPT $2p_{3/2} - 2s_{1/2}$ energies (au)

Term	Be-like	C-like	Ne-like
$E^{(0)}$	163.9885	164.7607	165.9570
$E^{(1)} + B^{(1)}$	2.4276	3.8185	5.7267
$E^{(2)}$	-0.0150	-0.0277	-0.0579
$B^{(2)}$	0.0081	0.0096	0.0011
Recoil	-0.0017	-0.0019	-0.0019
MBPT	163.3280	168.5592	171.6250

The QED corrections for these three ions are listed in Table 3. These corrections include the self-energy evaluated in the model potential and the vacuum-polarization from the Uehling potential. Additionally, Wichmann-Kroll and two-loop corrections taken from [6] are included. The individual contributions and their sums are listed in Table 3. In Table 4, we list experimental and MBPT energies, their differences (which are the experimental QED corrections), and the theoretical QED corrections from Table 3. The theoretical and experimental QED corrections are seen to agree at the 5%

Table 3: QED Corrections (au)

Term	Be-like	C-like	Ne-like
SE	-1.9730	-1.9358	-1.8812
Uehling	0.5654	0.5537	0.5366
WK+HO	-0.0276	-0.0270	-0.0262
QED	-1.4352	-1.4091	-1.3709

Table 4: Comparison of MBPT energies with experiment (eV)

Ion	Expt.	MBPT	Diff.	QED
Li	4459.37(27)	4498.81	-39.44(27)	-39.32
Be	4501.72(21)	4541.93	-40.21(21)	-39.05
C	4548.32(16)	4586.73	-38.41(16)	-38.34
F	4593.83(12)	4631.62	-37.79(12)	-37.30
Ne	4630.93(26)	4670.16	-39.23(26)	-37.30

level of accuracy, giving a test of the $n = 2$ Lamb shift, comparable to the test provided by the K-shell binding energies.

3.2 Copperlike Ions

The copper atom is the largest ion with a "complete" isoelectronic sequence. Copperlike ions have a closed core,

$$(1s)^2(2s)^2(2p)^6(3s)^2(3p)^6(3d)^{10},$$

and a single valence electron. Energy levels of copperlike ions are precisely and completely known; they are available for many ions in the sequence on the NIST online data base [22]. An analysis of the structure of copperlike ions carried out through third order in MBPT in Ref. [23] provides yet another test of the $n = 4$ Lamb shift. In each order of MBPT, the energy consists of a core contribution, which is the same for each valence state and a valence contribution. Starting our calculations in the DHF approximation, the lowest-order valence energy is just the DHF eigenvalue, ϵ_v. There is no first-order correction to the energy. The second- and third-order corrections to the valence energies are given by the sums

$$E_v^{(2)} = \sum_{amn} \frac{\tilde{v}_{mnav} v_{avmn}}{\epsilon_m + \epsilon_n - \epsilon_v - \epsilon_a} - \sum_{abm} \frac{\tilde{v}_{abmv} v_{mvab}}{\epsilon_m + \epsilon_v - \epsilon_a - \epsilon_b}, \tag{14}$$

$$E_v^{(3)} = \sum_{mabcd} \frac{\tilde{v}_{abvm} v_{cdab} v_{mvcd}}{(\epsilon_{ab} - \epsilon_{vm})(\epsilon_{cd} - \epsilon_{mv})} + 17 \text{ more terms.} \tag{15}$$

In these equations, the quantities v_{abcd} are two-electron Coulomb (or Coulomb plus Breit) matrix elements. The indices a, b, $\cdots$ at the beginning of the alphabet designate sums over occupied orbitals and the indices m, n, $\cdots$ refer to states (including continuum states) above the closed core. In practical calculations, we quantize the atom in a box of finite but large radius and replace the real spectrum in the box by a finite psuedospectrum constructed from B-splines. The second-order energy for a single state in a copperlike ion can be evaluated in a matter of minutes on a computer workstation. The third-order energy requires several hours; the evaluation of sums over four excited orbitals being the most time consuming part of the calculation. The results of our MBPT calculation for Cu-like tin (Z=50) are shown in Table 5. The perturbation expansion is seen to converge rapidly. In the lower panel of the table, we compare the theoretical intervals $4p_{3/2} - 4p_{1/2}$ and $4p_{3/2} - 4s_{1/2}$ with experiment. The former interval agrees with experiment to within the combined theoretical and experimental uncertainties. The $4p_{3/2} - 4s_{1/2}$, by contrast, is significantly different from experiment. Again, we attribute the difference to the $n = 4$ Lamb shift. In Fig. 9, we compare experimental and theoretical values for the $n = 4$ Lamb shift along the copper isoelectronic sequence. The theoretical values were determined in a local potential that approximates the DHF potential. As seen from the figure, the experimental and theoretical values agree at the 10% level of accuracy. Other similar tests of the Lamb shift at the 10% level of accuracy have been carried out in the lithium [24] and sodium [25] isoelectronic sequences.

3.3 Conclusions

The tests of the Lamb shift described above can be summarized as follows: the one-Loop strong-field $n = 1$ Lamb shift is tested to $\approx 5\%$ in K-shells of heavy atoms; the $n = 2$ Lamb shift is tested to $\approx 5\%$ in highly-charged uranium ions, and the $n = 4$ Lamb shift is tested to $\approx 10\%$ in copper-like ions. More precise tests in many-electron atoms require more accurate many-body calculations and consideration of correlation corrections to the Lamb shift.

Table 5: Energies (a.u.) of Sn^{+21}.

Term	$4s_{1/2}$	$4p_{1/2}$	$4p_{3/2}$
$E^{(0)}$	-23.56930	-21.91682	-21.48453
$E^{(2)}$	-0.06009	-0.06000	-0.05583
$E^{(3)}$	0.00406	0.00383	0.00355
$B^{(1)}$	0.01493	0.02117	0.01478
$B^{(2)}$	-0.00433	-0.00451	-0.00449
$B^{(3)}$	0.00017	0.00027	0.00019
Recoil	0.00009	0.00005	0.00005
E_{Tot}	-23.61488	-21.95601	-21.52627

	$p_{3/2} - p_{1/2}$	$p_{3/2} - s_{1/2}$
E_{Tot}	0.04297(2)	2.0883(3)
E_{Expt}	0.04303(3)	2.0807(1)

References

[1] S. Brenner and G. E. Brown, Proc. R. Soc. (London) **A218**, 422 (1953).

[2] W. R.. Johnson and K. T. Cheng, in *Atomic Inner-Shell Physics* ed. B. Crasemann (Plenum, New York, 1985), Chap. 1, pp. 1-29.

[3] J. A. Bearden and A. F. Burr, Rev. Mod. Phys. **39**, 125 (1967).

[4] C. W. de Jager, H. de Vries, and C. de Vries, At. Data and Nucl. Data Tables **14**, 479 (1974).

[5] R. Engfer, H. Schneuwly, J. L. Vuilleumier, H. K. Walter, and A. Zehnder, At. Data and Nucl. Data Tables **14**, 509 (1974).

[6] W. R. Johnson and G. Soff, At. Data and Nucl. Data Tables **33**, 405 (1985).

[7] I. Lindgren and J. Morrison, *Atomic Many-Body Theory* (Springer-Verlag, Berlin, 1982).

[8] B. T. Pickup and O. Goscinski, Mol. Phys. **26**, 1013 (1973).

[9] P. Indelicato and E. Lindroth, Phys. Rev. A**46**, 2426 (1992).

[10] J. B. Mann and W. R. Johnson, Phys. Rev. A**4**, 44 (1971).

[11] G. E. Brown, J. S. Langer, and G. W. Schaefer, Proc. R. Soc. (London) **A251**, 92 (1959).

[12] G. E. Brown and D. F. Mayers, Proc. R. Soc. (London) **A251**, 105 (1959).

[13] A. M. Desiderio and W. R. Johnson, Phys. Rev. A**3**, 1267 (1971).

[14] P. J. Mohr, Ann. Phys. (N.Y.) **88**, 26 ; **88**, 52 (1974).

[15] K. T. Cheng and W. R. Johnson, Phys. Rev. A**14**, 1943 (1976).

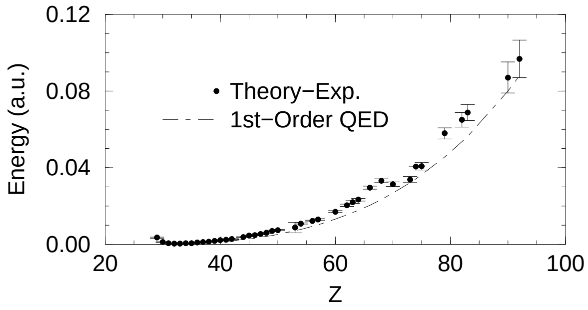

Figure 9: Comparison of "experimental" and theoretical values of the $4p_{3/2}-4s_{1/2}$ Lamb shift in copperlike ions.

[16] G. Soff, P. Schlüter, B. Muller, and W. Greiner, Phys. Rev. Lett. **48**, 1465 (1982).

[17] K.T. Cheng, W.R. Johnson, and J. Sapirstein, Phys. Rev. Lett. **66** 2962 (1991).

[18] S. A. Blundell and N. J. Snyderman, Phys. Rev. A**44**, R1427 (1991).

[19] I. Lindgren, H. Persson, S. Salomonson, and A. Ynnerman, Phys. Rev. A**47**, R4555 (1993).

[20] P. Beiersdorfer, D. Knapp, R. E. Marrs, S. R. Elliott, and M. H. Chen, Phys. Rev. Lett. **71**, 3939 (1993).

[21] W. R. Johnson, J. Sapirstein, and K. T. Cheng, Phys. Rev. A**51**, 297 (1995).

[22] J.R. Fuhr, W.C. Martin, A. Musgrove, J. Sugar, and W.L. Wiese, *NIST Atomic Spectroscopic Database* ver. 1.1 January 1996. NIST Physical Reference Data. Online. National Institute of Standards and Technology. Available http://physics.nist.gov/PhysRefData/contents.html

[23] W. R. Johnson, S. A. Blundell, and J. Sapirstein, Phys. Rev. A**42**, 1087 (1990).

[24] W. R. Johnson, S. A. Blundell, and J. Sapirstein, Phys. Rev. A**37**, 2764 (1988).

[25] W. R. Johnson, S. A. Blundell, and J. Sapirstein, Phys. Rev. A**38**, 2699 (1988).